MID-AMERICA TRANSPORTATION CENTER

Report # MATC-UI: 141-1

Final Report
WBS:25-1121-0005-141-1

Development of New Design Guidelines for Protection against Erosion at Bridge Abutments

George Constantinescu, Ph.D.
Professor
Department of Civil and Environmental Engineering
The University of Iowa

2018

A Cooperative Research Project sponsored by
U.S. Department of Transportation- Office of the Assistant Secretary for Research and Technology

Development of New Design Guidelines for Protection against Erosion at Bridge Abutments

George Constantinescu, Ph.D., PI
Professor
Department of Civil and Environmental Engineering
The University of Iowa

A Report on Research Sponsored by

Mid-America Transportation Center

University of Nebraska–Lincoln

July 2018

Technical Report Documentation Page

1. Report No. 25-1121-0005-141-1	2. Government Accession No.	3. Recipient's Catalog No.
4. Title and Subtitle Development of New Design Guidelines for Protection against Erosion at Bridge Abutments		5. Report Date July, 2018 6. Performing Organization Code
7. Author(s) George Constantinescu, Ph.D.; ORCID: 0000-0001-7060-8378		8. Performing Organization Report No.
9. Performing Organization Name and Address Department of Civil and Environmental Engineering, The University of Iowa, Iowa City, IA 52242		10. Work Unit No. 11. Contract or Grant No. 69A3551747107
12. Sponsoring Agency Name and Address		13. Type of Report and Period Covered Final Report May 2017-May 2018 14. Sponsoring Agency Code 91994-1

15. Supplementary Notes
Conducted in cooperation with the U.S. Department of Transportation, Federal Highway Administration.

16. Abstract

Over the last two decades, the United States Midwest has experienced increasingly catastrophic flood events. Severe erosion problems occurred even though the erosion protection design measures for bridge abutments and their embankments followed the existing guidelines (e.g., HEC 23, 2001 and following updates through 2009). The methodology proposed to estimate design variables in scour protection measure formulas (e.g., size of riprap stone) for these guidelines at such sites is oversimplified. The present research proposes a numerically-based approach for improving methodologies to design riprap protection measures at wing-wall and spill-through abutments. The mean flow fields and the bed shear stress distributions predicted using high-resolution, fully three-dimensional (3-D), non-hydrostatic RANS simulations were used to estimate the maximum bed shear stress over the riprap layer, the shear-failure entrainment threshold for the riprap stone and the other variables in the design formulas recommended in HEC 23 (Lagasse et al., 2001). The numerically-based approach was successfully validated for the case of wing-wall abutments placed in a straight channel. Simulations were also conducted for spill-through abutments with varying floodplain width, ratio of abutment length to floodplain width, and riprap stone size. The simulations demonstrated the critical Froude number corresponding to the entrainment threshold decreases monotonically with increasing L_a/B_f or L_a/y_f (B_f=floodplain width, L_a=abutment length, y_f=flow depth over floodplain). Modifications are proposed to the standard Lagasse et al. (2001) formula that ensure the (modified) design formula is applicable to a range of flow and geometrical parameters. There is a need for further research to determine the range of applicability of the standard design formulas such that they can be applied to more complex cases.

17. Key Words Bridges, Bridge scour, Bridge abutment, Local Scour, Rip-rap protection against scour	18. Distribution Statement No restrictions. This document is available through the National Technical Information Service, Springfield, VA 22161.		
19. Security Classif. (of this report) Unclassified	20. Security Classif. (of this page) Unclassified	21. No. of Pages 37	22. Price

Table of Contents

List of Figures

List of Tables

Acknowledgments

We would like to thank Prof. Bruce Melville form University of Auckland, New Zeeland for providing additional information on his experiments carried for wing-wall abutments.

Disclaimer

The contents of this report reflect the views of the authors, who are responsible for the facts and the accuracy of the information presented herein. This document is disseminated in the interest of information exchange. The report is funded, partially or entirely, by a grant from the U.S. Department of Transportation's University Transportation Centers Program. However, the U.S. Government assumes no liability for the contents or use thereof.

Abstract

Over the last two decades, the United States Midwest has experienced increasingly catastrophic flood events. Severe erosion problems occurred even though the erosion protection design measures for bridge abutments and their embankments followed the existing guidelines (e.g., Hydraulic Engineering Circular HEC 23, 2001 and following updates through 2009). The methodology proposed to estimate design variables in scour protection measure formulas (e.g., size of riprap stone) for these guidelines at such sites is oversimplified. The calibration of these formulas is based on a limited series of laboratory experiments conducted for a limited range of relevant geometrical and flow parameters that cause erosion at such bridge sites. This project aims to improve designs to increase erosion protection guideline applications.

The present research proposes a numerically-based approach for improving methodologies to design riprap protection measures at wing-wall and spill-through abutments. Such abutments are common at the floodplain on small bridges where no piers are present. The mean flow fields and the bed shear stress distributions predicted using high-resolution, fully three-dimensional (3-D), non-hydrostatic RANS simulations were used to estimate the maximum bed shear stress over the riprap layer, the shear-failure entrainment threshold for the riprap stone and the other variables in the design formulas recommended in HEC 23 (Lagasse et al., 2001). The numerically-based approach was successfully validated for the case of wing-wall abutments placed in a straight channel, for which detailed laboratory experiments are available. Simulations were also conducted for spill-through abutments with varying floodplain width, ratio of abutment length to floodplain width, and riprap stone size. The simulations demonstrated the critical Froude number corresponding to the entrainment threshold decreases monotonically with increasing L_a/B_f or L_a/y_f (B_f=floodplain width, L_a=abutment length, y_f=flow depth over

floodplain). Modifications are proposed to the standard Lagasse et al. (2001) formula that ensure the (modified) design formula is conservative enough when applied for the range of flow and geometrical parameters considered in the present study. There is a need for further research to determine the range of applicability of the Lagasse et al. (2001) formula and eventual modifications of the standard formula such that it can be applied to more complex cases (e.g., abutments placed in a curved channel).

Chapter 1 Introduction

1.1 Motivation

Over the last several decades, the United States has experienced increasingly severe flood events (e.g. during 1993 and 2008) both in terms of frequency and intensity (e.g. peak discharges and stages, duration of the flood event). Consequently, significant erosion can occur if piers, abutments and bridge embankments are not protected effectively. This is especially a concern in the US Midwest where a large number of small bridges are present in rural areas. In extreme cases including large floods when overtopping occurs, the embankments of such small bridges can be washed away. The most common type of protection measure is to place riprap stone in regions around the base of the structure where severe scour is expected to develop. The increased size/weight of the riprap stones enables them to resist the increased velocities and turbulence caused by the presence of the abutment in the flow, and thereby provide an armor layer protection to the underlying sediments. Riprap placed in an apron at the base of an abutment may be subjected to shear failure. Shear failure occurs where the individual riprap stones are not large enough to resist entrainment by the flow. Two common types of abutments encountered at small bridges are spill-through and wing-wall abutments.

An example is shown in figure 1.1, where the flood washed the back sides of the two wing-wall abutments during the 1993 flood at a small Iowa bridge. After the flood, the embankment was reconstructed by filling the washed road reaches in the vicinity of the bridge and protecting the top surfaces with riprap stone.

Figure 1.1 Effect of flood on erosion at a small bridge with two (wing-wall) abutments situated in Squaw Creek, close to Ames (Iowa).

The first two pictures show all the erodible material behind the toe of the abutment washed by the flood. The last two pictures show the bridge after the abutments were reconstructed and large-scale riprap stone was placed on the floodplain around the abutments for protection against future floods. These infrastructural failures highlight the need for increased attention on abutment design for small bridges where the abutments are placed on the floodplain and no piers are present.

Existing design guidelines are mostly based on laboratory experiments (flume studies) conducted for a few types of such abutments (e.g., in terms of shape, geometry, construction

materials) and for a limited range of flow conditions. For example, present design guidelines are not accounting for pressure scour effects at high flow conditions when the bridge deck becomes submerged. Severe erosion problems were reported at some bridge abutments where riprap protection measures followed existing design guidelines. These guidelines need to be improved by proposing modified formulas or methodologies that can provide effective protection against erosion for a wider range of flow and geometrical conditions at these two types of abutments (HEC 23, Lagasse et al., 2001, Melville and Coleman, 2000, Melville et al., 2006a, 2006b, Hoffmans and Verheij, 1997, Ettema et al., 2011).

1.2 Objectives

As discussed in section 1.1, there is a clear need to conduct new research to better address the fundamental aspects of the scour protection design guidelines for abutments in HEC 23. The main research objectives of this project are to:

1. Validate a numerical approach based on 3-D RANS non-hydrostatic simulations to estimate maximum bed shear stress and to evaluate the critical Froude number at which entrainment of riprap stone with a certain diameter will occur
2. Test performance of main design formula recommended by HEC 23 (Lagasse et al., 2001) to estimate minimum size of riprap stone used for protection against erosion for wing-wall and spill-through abutments placed in straight channels with a floodplain
3. Propose modified versions of the design formula such that it can be applied for a wider range of flow and geometrical parameters

In a more general context, the main impact of the present research will be to get a better understanding of why existing riprap design formulas are not conservative enough in some cases

and on ways to improve the performance of these formulas (e.g., via inclusion of additional factors of safety, different estimation of some of the variables in existing design formulas) in order to reduce the risk of a serious bridge failure due to flood-induced scour.

1.3 Justification of Research Approach

Understanding and being able to quantitatively describe how the hydrodynamics of the stream flow field (velocity magnitude and bed shear stress distributions around the bridge site) changes with increasing stage and discharge as a result of a flood is critical to be able to propose effective measures to protect bridge abutments and piers against erosion. The National cooperative Highway Research Program Report 587 used in the development of HEC 23 states the following:

> Selection of countermeasures to protect bridges from scour requires estimates of velocity distributions in the bridge opening. Estimates of the peak velocity in what is typically a highly non-uniform flow distribution near the tip of the abutment is necessary to determine whether countermeasures are necessary and, if so, to determine the type, size, and extent of countermeasures to protect bridge abutments from scour. Laboratory physical models have been developed to determine the size, type, and location of protection for a relatively small range of flow conditions at bridges; however, the laboratory models represent very simplistic geometric conditions. Effective transfer of laboratory model results to the complex hydrodynamic conditions of real bridge sites requires that flow velocity be predicted in the vicinity of bridge abutments using numerical models.

The report also comments on the limitations of the two-dimensional (2-D) depth-averaged modeling approach which was used to provide more accurate estimations of the variables in the design formulas used to protect against erosion. The main limitations of the 2-D approach are due to the hydrostatic pressure assumption and simplified turbulence modeling. Moreover, the region of maximum velocity amplification near the abutment toe is generally

located in a region of high flow curvature and, in many cases, it is situated over a sloped surface where such 2-D numerical simulations give relatively large errors.

The present study uses fully three-dimensional (3-D) RANS simulations performed on fine meshes to obtain the velocity flow field. This allows direct estimation of the boundary shear stress over the whole bed region, including over the layer of riprap. For each set of geometrical and flow conditions, the 3-D RANS simulation results are then used to predict the maximum shear stress over the riprap region. This bed shear stress is then compared with the critical value for riprap failure given a certain mean size of the riprap stone following the approach of Melville and Coleman (2000) and Melville et al. (2007) to determine if riprap failure will occur or not. In particular, this methodology can be used to test the performance of the leading design formulas recommended by HEC 23 for erosion protection of bridge abutments using riprap stone.

The proposed approach is very general and can be applied for more complex planform geometries (e.g., curved channels) and for bridge sites with geometrical complexities (e.g., spur dikes present at the channel bank, etc.). Especially for such cases, laboratory experiments are very expensive and the range of geometrical (e.g., channel aspect ratio, width of the floodplain) and flow parameters in these experiments is even more limited compared to the simpler case of an abutment placed in a straight channel. The numerical-based approach adopted in the present study does not face these limitations. Moreover, this approach can also be applied for cases when pressure scour effects are significant, something that is impossible to be achieved using 1-D and 2-D numerical models.

Chapter 2 Numerical Method

STAR-CCM+ is a state-of-the-art commercial code developed by CD-Adapco which solves the fully 3-D non-hydrostatic Navier-Stokes equations using the finite volume method on structured/unstructured meshes. The mean effect of turbulence on the momentum is accounted for by including an additional viscosity term called eddy viscosity.

$$\frac{\partial U_i}{\partial x_i} = 0 \tag{2.1}$$

$$\frac{\partial U_i}{\partial t} + \frac{\partial (U_i U_k)}{\partial x_k} = -\frac{1}{\rho}\frac{\partial P}{\partial x_i} + \frac{1}{\rho}\frac{\partial}{\partial x_k}\left[(\mu + \mu_t)\left(\frac{\partial U_i}{\partial x_k} + \frac{\partial U_k}{\partial x_i}\right)\right] - g\hat{k} \tag{2.2}$$

where U_i = Reynolds Averaged velocity component along the i direction based on the original velocity component

u_i, ρ = density of the fluid

μ = molecular dynamic viscosity

μ_t = eddy viscosity calculated from the RANS turbulence model

P = pressure

g = gravity

$\hat{k}$ = unit normal vector along the vertical direction

The RANS equations are solved based on a finite volume representation. The advective terms are discretised using a second-order accurate in a space upwinding scheme, while the transient term was second-order accurate based on an implicit representation. The diffusive term and the pressure gradient term are discretised using a second-order central difference scheme.

The pressure-coupling algorithm chosen was the SIMPLE algorithm. In the SIMPLE algorithm, the RANS equations are solved and an intermediate velocity is obtained which does not satisfy the continuity, or mass conservation equation. A pressure-correction algorithm is employed to modify the pressure field, in turn modifying the mass fluxes and velocity fields in order to satisfy mass conservation.

The realizable two-layer k-ε turbulence model and the k-ω SST models were chosen to perform the RANS simulations. The SST model performed more accurately for channel flow simulations with a large value of the relative bed roughness, leading to its use in the simulations of flow-past abutments. STAR CCM+ with the SST turbulence model was widely used and validated for predictions of flow in channels containing hydraulic structures (Cheng et al., 2018), including for cases when an unsteady flood wave advanced in a channel with natural bathymetry (Cheng et al., 2018 and Horna-Munoz and Constantinescu, 2016, 2017).

No-slip boundary conditions were specified at all wall boundaries, whereas the outlet was specified as a pressure outlet boundary. The bed shear was calculated using the law of the wall for rough or smooth surfaces. The surface roughness k_s is different in the riprap region and over the rest of the channel bed containing a layer of sand. The abutment walls were treated as smooth surfaces. The free surface was treated as a slip boundary with zero vertical velocity. Preliminary straight channel flow, steady RANS simulations with periodic boundary conditions in the streamwise direction were performed to obtain a fully developed channel flow solution. The cross section of the periodic channel was identical to the inlet section of the computational domain containing the abutment (a floodplain was placed in the vicinity of the main channel). This fully developed 2-D velocity field and the turbulence variables were specified at the inlet of the domain containing the abutment.

STAR-CCM+ contains a very powerful meshing capability in which an initial geometry can be imported, smoothed in such a way to improve computational efficiency, and to obtain better results without loss of information. Once the geometry has been processed, a volume mesh is created with the desired meshing model to obtain a high quality mesh. Some meshing models include tetrahedral, hexahedral, and polyhedral models with mesh refinement near boundaries. Additional refinement can be included near boundaries by producing high-aspect ratio, highly skewed cells named prism layers. One of the main advantages of this software is that it allows automatic grid refinement in critical regions (e.g., boundary layers) around hydraulic structures (e.g., abutments). Thus, high quality meshes are easy to generate in very complex domains and the amount of time needed to generate such meshes is relatively small.

Chapter 3 Wing-Wall Abutments

3.1 Description of Test Cases and RANS Solutions

Wing-wall abutments simulations were performed with different values of the riprap mean stone diameter and for two different flow depths corresponding to normal flow and flood conditions (flow over the floodplain) and four different values of the riprap diameter $D_{50riprap}$ (20 mm, 28 mm, 40 mm, and 60 mm). The main geometrical dimensions (B_f=floodplain width, L_a=abutment length, y_m=flow depth over main channel, y_f=flow depth over floodplain, R2, R3 and R4) and mean sediment size diameter inside the channel and the riprap layer are summarized in table 3.1 for the eight test cases.

Table 3.1. Matrix of test cases considered for the wing-wall abutment

		Ym (m)	Yf (m)	Bf (m)	R1 (m)	R2 (m)	R3 (m)	R4 (m)	D50-sand (mm)	D50-riprap (mm)	$U_{shear\text{-}failture}$ *
Case I	a	0.10	0.00	0.00	0.25	0.60	0.50	0.20	0.82	40	0.175
CaseII	a	0.17	0.07	0.40	0.25	0.60	0.50	0.20	0.82	20	0.120
	b	0.17	0.07	0.40	0.25	0.60	0.50	0.20	0.82	28	0.145
	c	0.17	0.07	0.40	0.25	0.60	0.50	0.20	0.82	40	0.175
	d	0.17	0.07	0.40	0.25	0.60	0.50	0.20	0.82	61	0.210
Case III	a	0.17	0.07	1.40	0.25	0.60	0.50	0.20	0.82	20	0.120
	b	0.17	0.07	1.40	0.25	0.60	0.50	0.20	0.82	40	0.175
	c	0.17	0.07	1.40	0.25	0.60	0.50	0.20	0.82	61	0.210
$U_{shear\text{-}failture}=U_{tau\_critical}*0.35/U_{ref}$ U_{ref}=0.4											

Also indicated in Table 3.1 is the non-dimensional value of the critical bed shear stress for shear failure for the riprap.

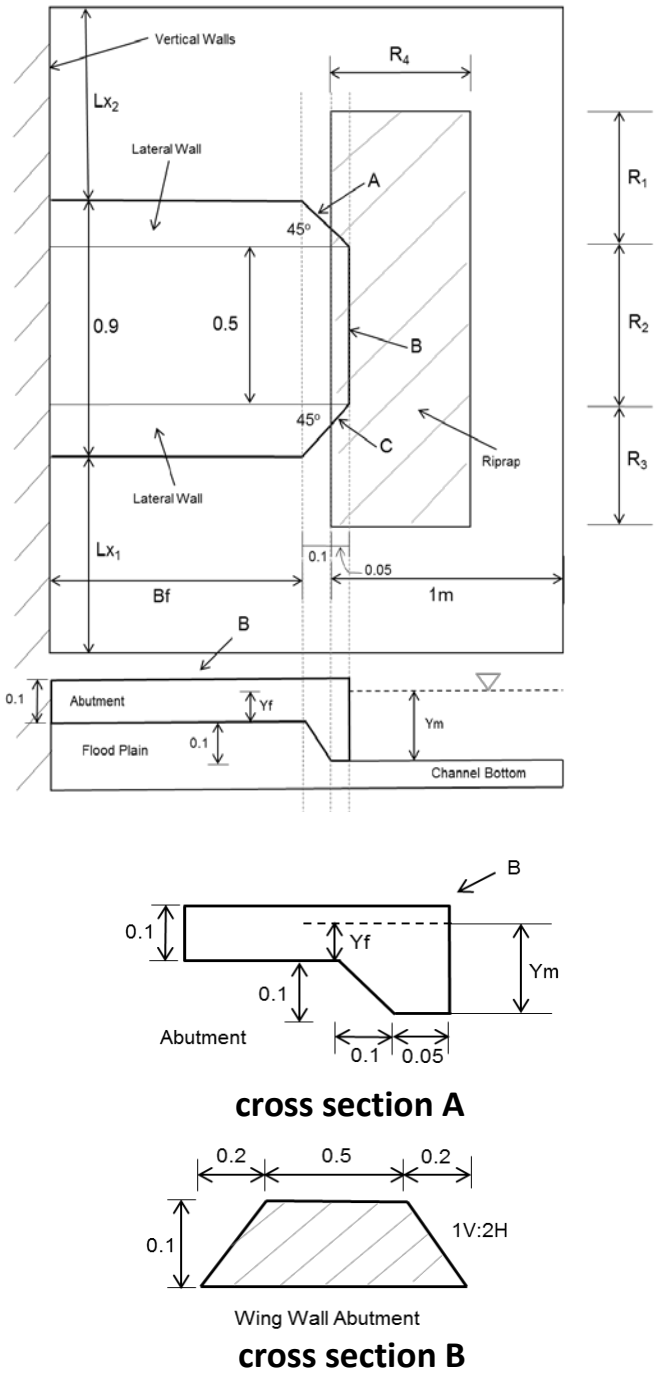

Figure 3.1 Sketch showing general layout of the numerical simulations performed for a wing-wall abutment placed on the floodplain of a straight channel. Dimensions are in meters.

Figure 3.1 shows a sketch of the general layout of the computational domain, the main geometrical variable, and the overall shape of the wing-wall abutment. The bottom frames show two cross sections cutting through the abutment. The wing-wall abutment geometrical set up corresponds to that used in the laboratory experiments of Melville et al. (2007).

Figure 3.2 provides more information on the computational domain used in the simulations conducted with different values of the floodplain width, B_f=0.0 m (Case I), B_f=0.4 m (Case II) and Bf=1.4 m (Case III). Outside of the riprap layer region, the flat channel bed was covered with sand with a mean diameter D_{50}=0.82 mm. The velocity scale was U_{ref}=0.4 m/s, while the length scale was L_{ref}=0.1 m for all simulations.

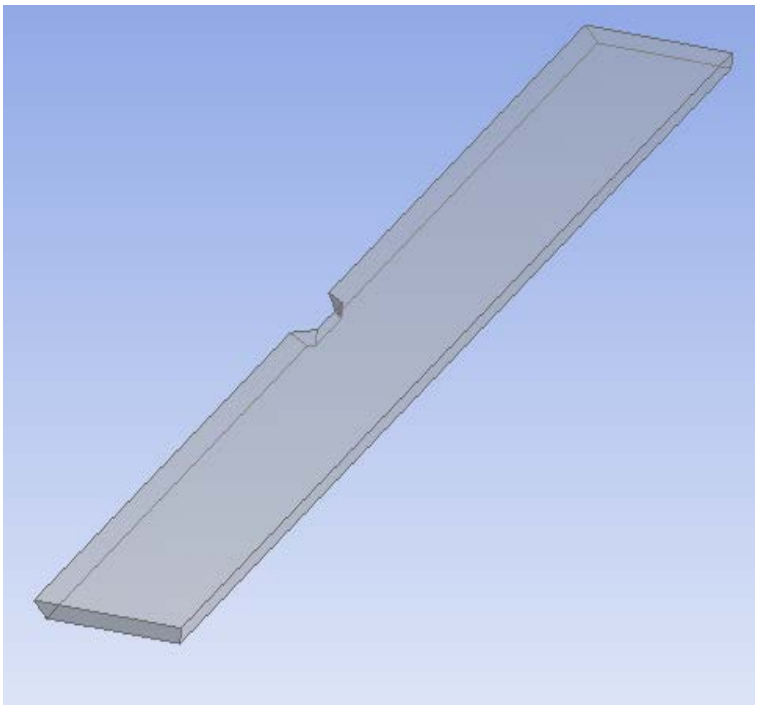

CASE I

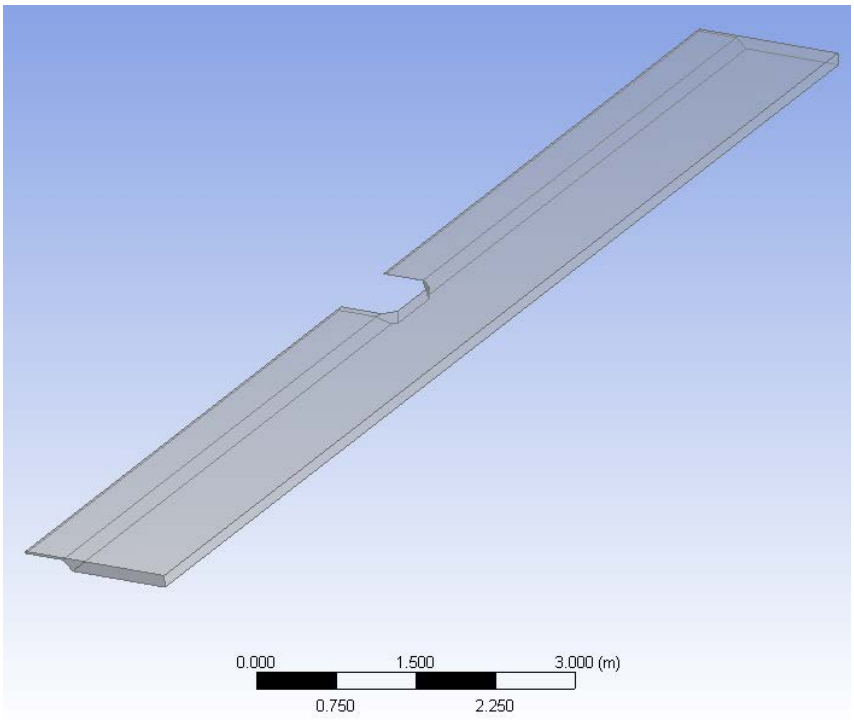

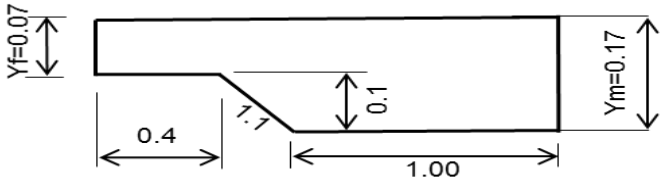

CASE II

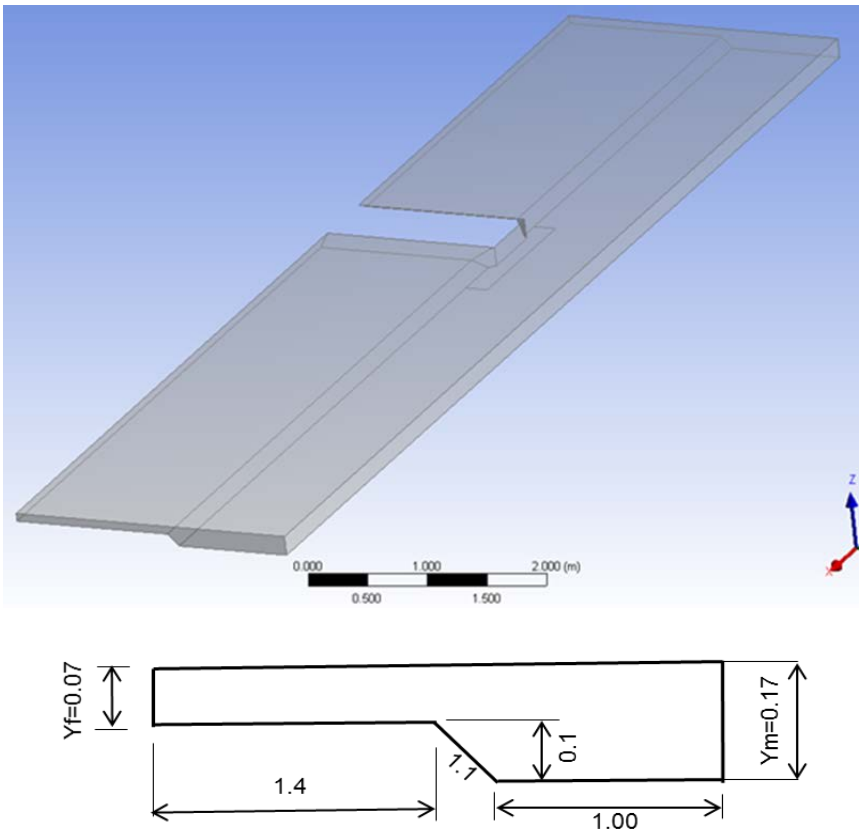

CASE III

Figure 3.2 Computational domain used in Case I, Case II, and Case III simulations of flow past a wing-wall abutment. Shown are the main lengths (m) in the channel cross section.

These test cases correspond to the main test cases considered in the experimental laboratory study of Melville et al. (2007). The numerical simulations were used to determine the distribution of the depth-averaged velocity and of the bed shear stresses around the abutment and the locations where the maximum bed shear stress, root-mean-square of the bed shear stress, mean horizontal velocity, and turbulent kinetic energy (TKE) occur.

Figure 3.3 shows a view of the computational mesh.

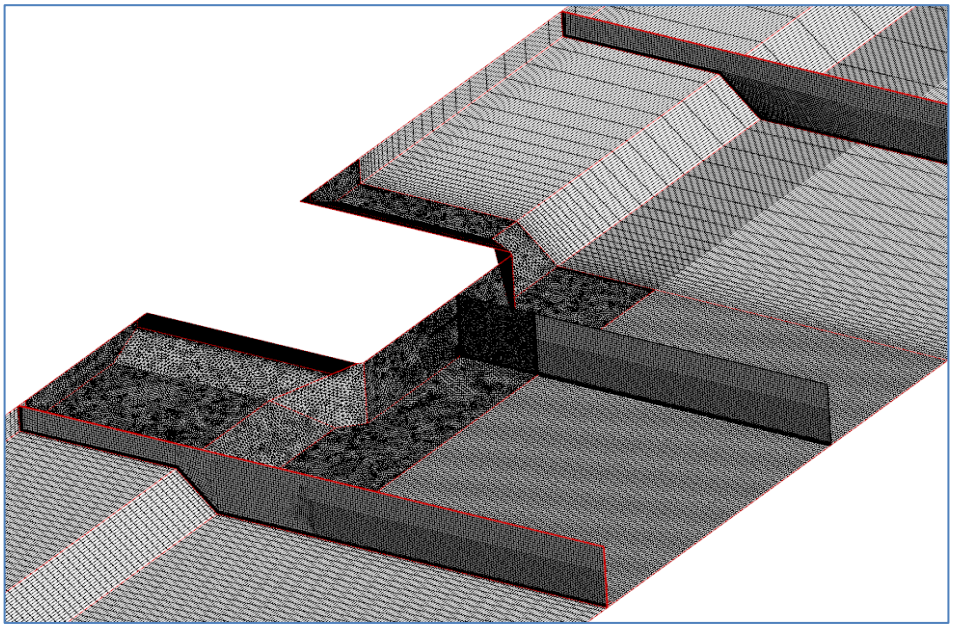

Figure 3.3 Grid used to mesh the channel containing a wing-wall abutment for Case II simulations.

For most simulations, the total number of computational cells was close to two million. The mesh was refined close to all solid boundaries, including the abutment surfaces, to insure all the boundary layers were sufficiently well resolved. This is essential to accurately predict the mean flow and bed friction velocity distributions. The mesh around the abutment was unstructured. It was connected to a structured mesh upstream and downstream of the abutment and also in the main channel, away from the toe of the abutment. To save computational resources, only half of the channel was simulated. The experiments were also performed in a similar geometrical set up. For each test case, simulations were conducted for flow conditions (mean velocity in the incoming channel or, equivalently, the Froude number in the section cutting through the

center of the abutment) corresponding to no shear failure and to shear failure of the riprap protection based on the experiments of Melville et al. (2007). For each test case two simulations were run with Froude numbers corresponding to no entrainment and entrainment of riprap, respectively.

Figure 3.4 shows the main characteristics of the flow past a spill-through abutment for the case the floodplain width is 0.4 m.

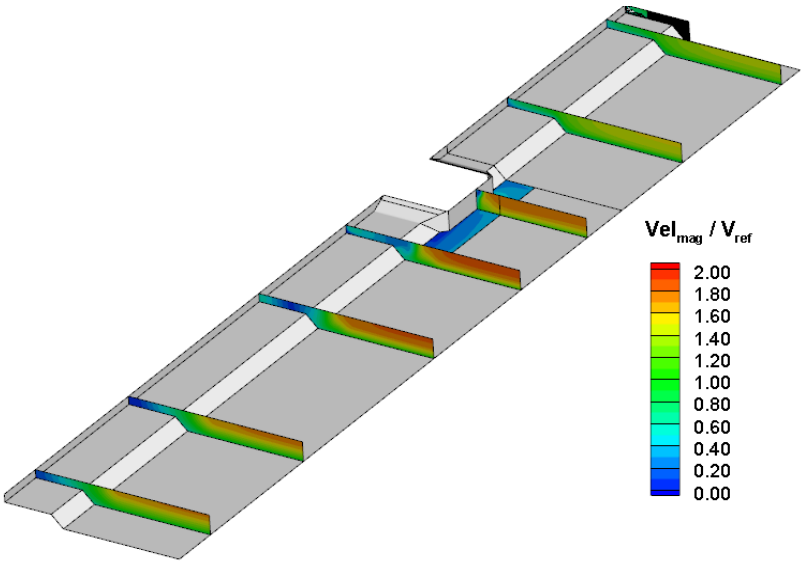

a)

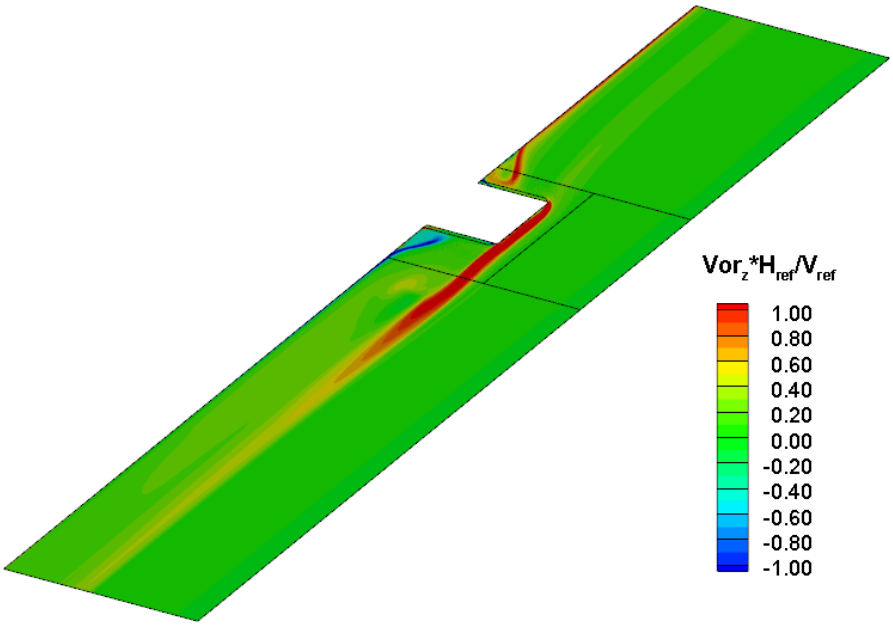
Vor$_z$*H$_{ref}$/V$_{ref}$
1.00
0.80
0.60
0.40
0.20
0.00
-0.20
-0.40
-0.60
-0.80
-1.00

b)

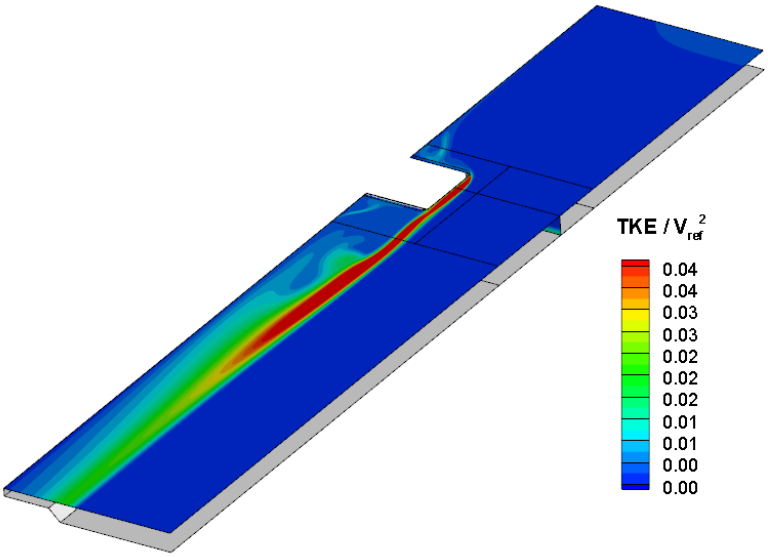
TKE / V$_{ref}^2$
0.04
0.04
0.03
0.03
0.02
0.02
0.02
0.01
0.01
0.00
0.00

c)

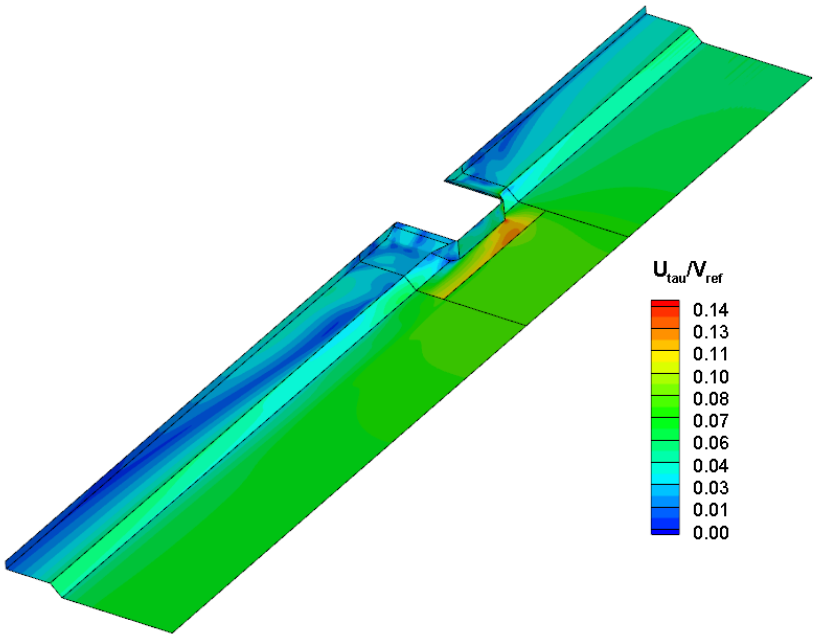

d)

Figure 3.4 Visualization of the solution for Case IIc simulation with Fr=0.65. a) nondimensional streamwise velocity in relevant cross sections; b) nondimensional vertical vorticity at the free surface; c) nondimensional TKE; d) nondimensional bed friction velocity.

As expected, the flow velocity is amplified in the cross sections cutting through the abutment and a large recirculation region forms close to the free surface, downstream of the abutment. The velocities over the floodplain are relatively small at all cross sections. As opposed to abutments placed in channels with no floodplain, the main separated shear layer (SSL) forming at the upstream edge of the toe of the abutment remains parallel and close to the toe of the abutment and the interface between the main channel and the floodplain (fig. 3.4b). Other regions of high vorticity correspond to the outer sides of the two recirculation regions forming upstream and downstream of the abutment, as the incoming flow passes the abutment. The main SSL is also a region of high turbulence production, as observed from the TKE distributions in figure 3.4c. Relatively large TKE values are also predicted in the downstream recirculation

region forming over the floodplain. The largest bed friction velocities are observed over the riprap layer. This is expected due to the much higher value of the bed roughness in this region and the fact that the riprap layer is placed inside the main channel where the flow velocities are larger. The bed friction velocity increases with the bed roughness. Relatively low values of the bed roughness are predicted over the floodplain even outside the two recirculation regions, mainly because the velocity magnitude is smaller in regions of reduced flow depth (fig. 3.4d).

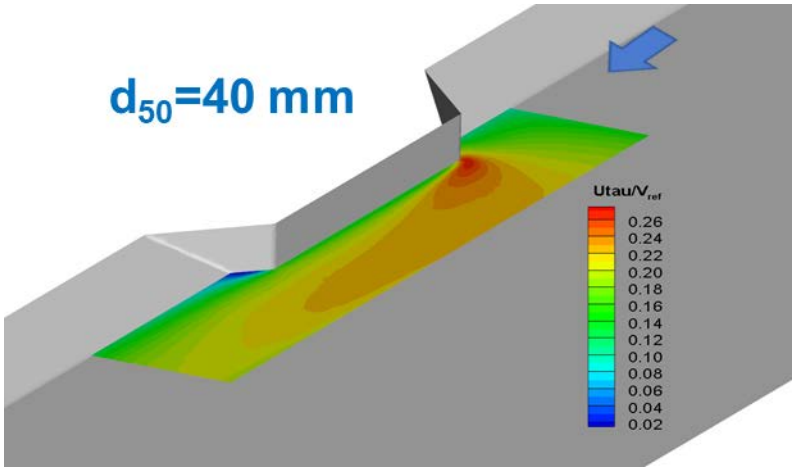

Case Ia

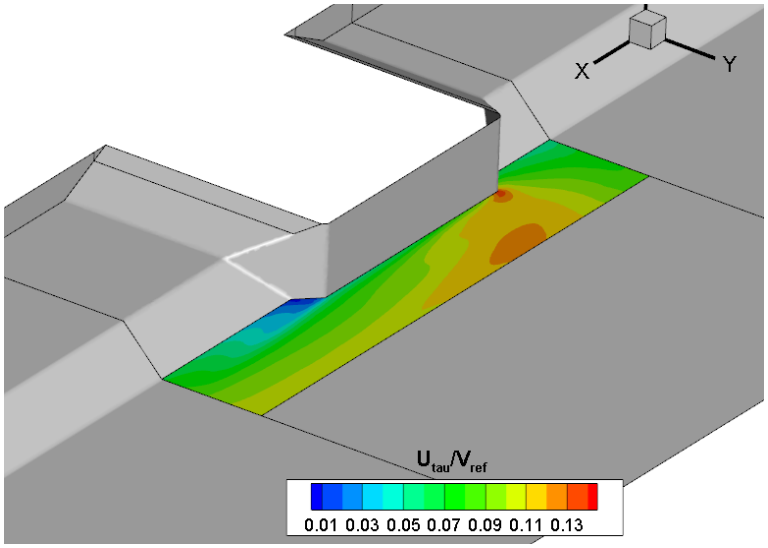

Case IIb

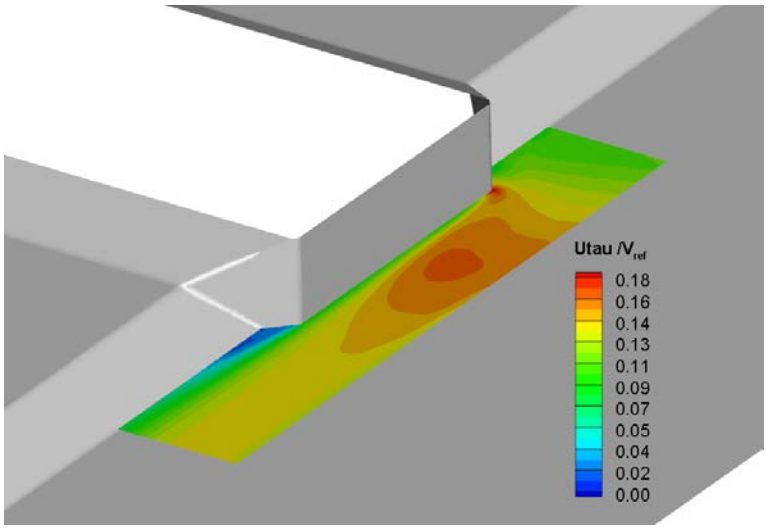

Case IIIb

Figure 3.5 Nondimensional bed friction velocity distribution over the riprap layer predicted by the numerical simulations for some of the wing-wall abutment test cases.

Figure 3.5 shows sample predicted distributions of the non-dimensional bed friction velocity over the riprap layer for wing-wall abutments. The relative position of the maximum value of the bed friction velocity is a function of the floodplain width. While in some cases the maximum value is close to the upstream edge of the abutment toe, in cases with a large floodplain width the maximum bed friction velocity value over the riprap region is predicted close to the symmetry plane of the abutment.

The inlet discharge was varied until the maximum value of the bed friction velocity in this region was slightly lower and slightly larger than 0.35 u_{*cr}, where u_{*cr} is obtained from the Shields diagram for a given mean diameter of the riprap, $D_{50riprap.}$ Following, Melville and Coleman (2000), this value was used to determine the riprap shear failure entrainment threshold. The Froude number, Fr, was calculated using the mean velocity in the section containing the abutment and the flow depth in the main channel for cases with $L_a=B_f$ (e.g., wing-wall abutments).

3.2 Validation

Simulations were conducted with flow solely inside the main channel (y_m=0.1 m) and with flow over the floodplain (y_m=0.17 m, y_f=0.07 m) for B_f=0.4 m and 1.4 m and for 20 mm<$D_{50riprap}$<61 mm. Five test cases for the wing-wall abutment corresponded to those in the experiments of Melville et al. (2007).

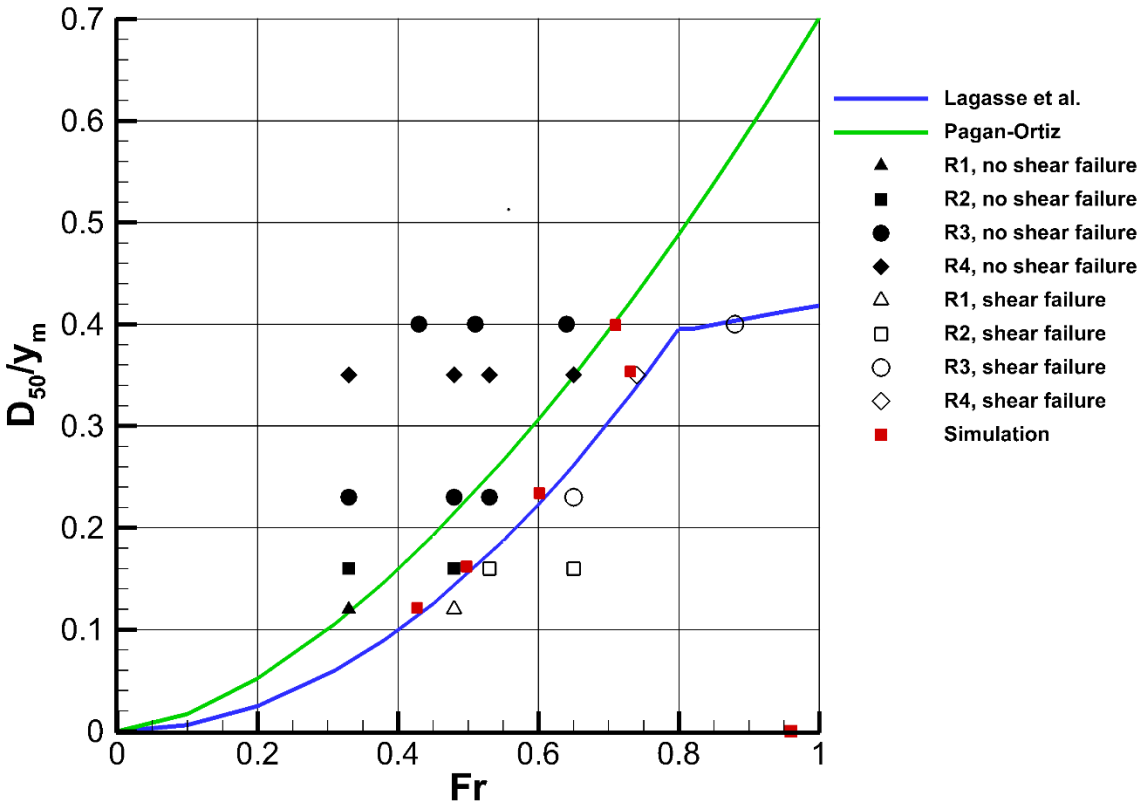

Figure 3.6 Comparison of numerical results with Lagasse et al. (2001) and Pagan-Ortiz (1991) equations and the experimental data of Melville et al. (2007) for wing-wall abutments. Simulation data show predicted conditions for threshold of riprap entrainment by shear failure. Experimental data show if failure occurred (open symbols) or not (solid symbols) in the corresponding experiments.

Figure 3.6 shows that for each of the five series of experiments, the numerically predicted shear failure entrainment threshold is situated in between the limiting experiments where no shear failure and shear failure were observed. This result is of great importance as it directly validates the proposed numerical approach to determine the entrainment threshold. Also shown are the predictions given by the design formulas of Pagan-Ortiz (1991) and Lagasse et al. (2001) that will be discussed more in depth in the next subchapter.

3.3 Comparison with Predictions of Design Formulas

Figure 3.7 shows additional numerical results for wide wing-wall abutments with B_f=1.4 m. Also represented are the design formula predictions of Pagan-Ortiz (1991)

$$D_{50}/y=(1.064/(S_s-1))^{0.81} * Fr^{1.62} \quad (3.1)$$

and the design formula predictions of Lagasse et al. (2001)

$$D_{50}/y=(K_s/(S_s-1))*Fr^{\alpha}\ w \quad (3.2)$$

where K_s = shape factor

for Fr<0.8, K_s=1.02 and α=2

for Fr>0.8, K_s=0.69 and α=0.28

S_s = specific gravity of riprap = 2.65

y = y_m for wing-wall abutments

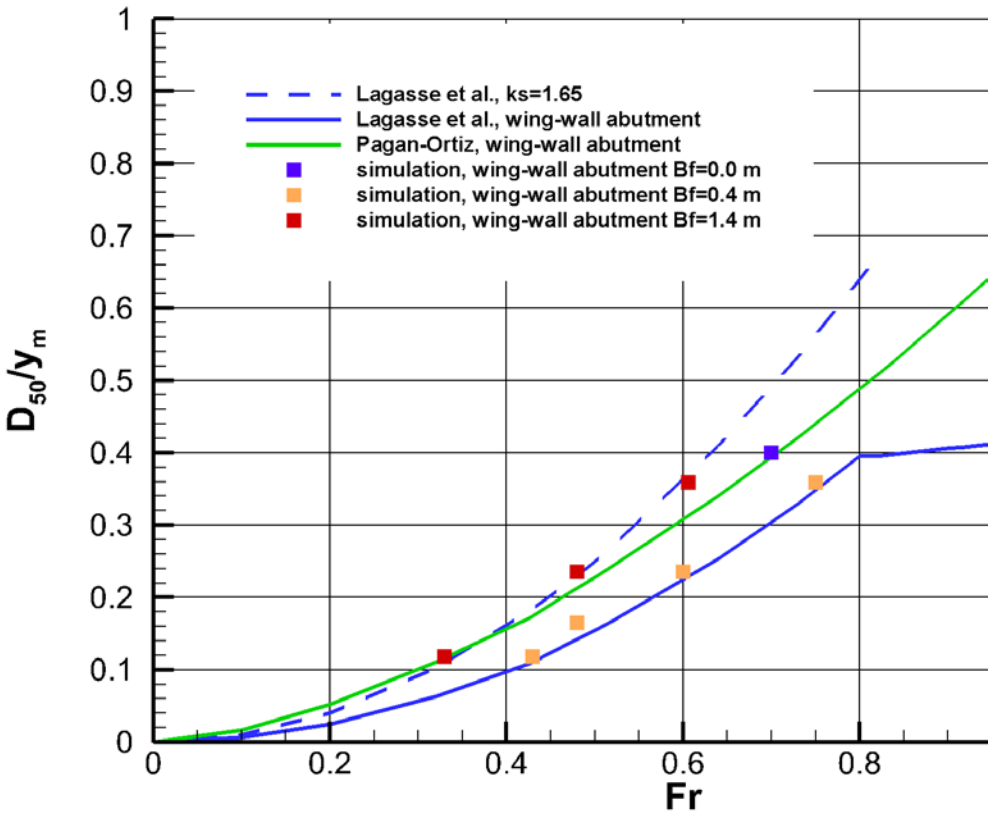

Figure 3.7 Comparison of numerical results with Lagasse et al. (2001) and Pagan-Ortiz (1991) equations and the experimental data of Melville et al. (2007) for wing-wall abutments. Plotted is a modified version of Lagasse et al. (2001) formula (K_s=1.65) that results in conservative predictions of minimum riprap size for analyzed cases with wide floodplains.

The Lagasse et al. (2001) formula does a great job for the high-flow cases with narrow floodplains (B_f=0.4 m), while Pagan-Ortiz (1991) accurately predicts the entrainment threshold for cases where the floodplain is not flooded. Neither formula is conservative enough for high-flow cases with wide floodplains (B_f=1.4 m). For such cases, using Lagasse et al. (2001) formula with a larger value of K_s=1.65 (Fr<0.8) results in agreement with the numerical experiments. These results show that the original Lagasse et al. (2001) formula is conservative enough only for high-flow cases with relatively narrow floodplains.

Chapter 4 Spill-Through Abutments

4.1 Description of Test Cases and RANS Solutions

Based on the experiments conducted by Melville et al. (2006) for spill-through abutments, eight test cases with y_m=0.17 m, y_f=0.07 m, B_f=1.0 m and 1.4 m, and $0.3<L_a/B_f<1$ were conducted with $D_{50riprap}$=40 mm and D_{50}=0.89 mm. Four simulations with B_f=1.4 m were conducted with $D_{50riprap}$=20 mm. For all cases, the width of the riprap layer was W=0.35 m (fig. 4.1).

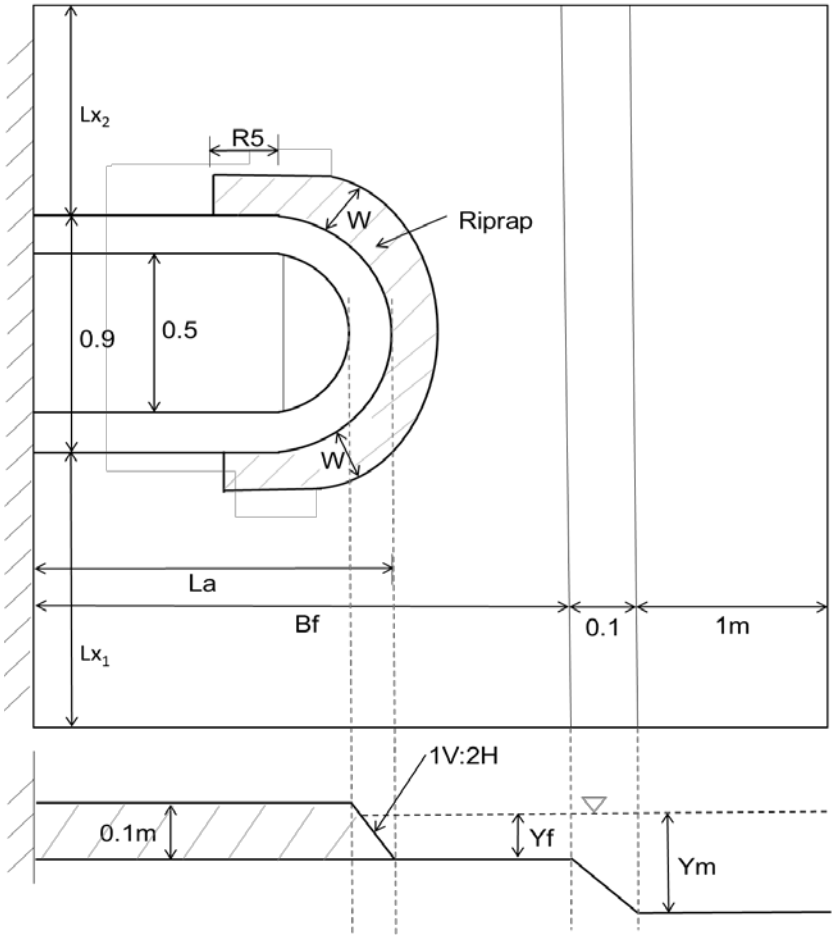

Figure 4.1 Sketch showing general layout of the numerical simulations performed for a spill-through abutment placed on the floodplain of a straight channel. Dimensions are in meters.

Table 4.1 summarizes the main geometrical parameters of these test cases.

Table 4.1. Matrix of test cases considered for the spill-through abutment

		Ym (m)	Yf (m)	Bf (m)	La (m)	R5(m)	W	D50-sand (mm)	D50-riprap (mm)	$U_{shear\text{-}failture}$ *
Case I	a1	0.17	0.07	0.50	0.50	0.35	0.35	0.82	20	0.120
	a2	0.17	0.07	0.50	0.50	0.35	0.35	0.82	40	0.175
CaseII	a1	0.17	0.07	1.00	0.50	0.35	0.35	0.82	20	0.120
	a2	0.17	0.07	1.00	0.50	0.35	0.35	0.82	40	0.175
	b1	0.17	0.07	1.00	0.70	0.35	0.35	0.82	20	0.120
	b2	0.17	0.07	1.00	0.70	0.35	0.35	0.82	40	0.175
	c1	0.17	0.07	1.00	1.00	0.35	0.35	0.82	20	0.120
	c2	0.17	0.07	1.00	1.00	0.35	0.35	0.82	40	0.175
Case III	a1	0.17	0.07	1.40	0.49	0.35	0.35	0.82	20	0.120
	a2	0.17	0.07	1.40	0.49	0.35	0.35	0.82	40	0.175
	b1	0.17	0.07	1.40	0.70	0.35	0.35	0.82	20	0.120
	b2	0.17	0.07	1.40	0.70	0.35	0.35	0.82	40	0.175
	c1	0.17	0.07	1.40	0.98	0.35	0.35	0.82	20	0.120
	c2	0.17	0.07	1.40	0.98	0.35	0.35	0.82	40	0.175
	d1	0.17	0.07	1.40	1.40	0.35	0.35	0.82	20	0.120
	d2	0.17	0.07	1.40	1.40	0.35	0.35	0.82	40	0.175

Figure 4.2 shows the whole computational domain for the case with B_f=1.4 m (Case III simulations) together with a cross-section. Also included are additional test cases relevant for understanding how the different flow and geometrical parameters affect the minimum required size of the riprap stone needed to avoid shear failure at spill-through abutments.

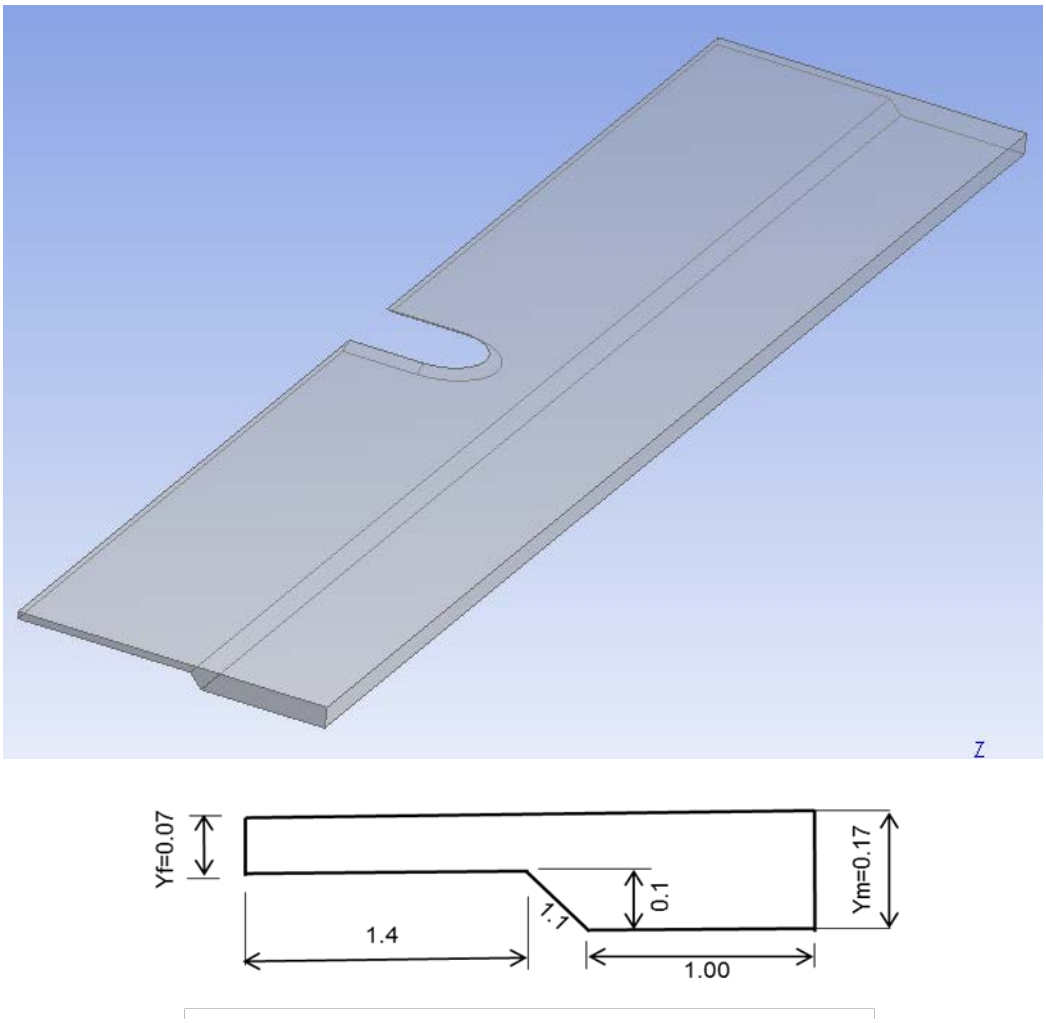

Figure 4.2 Computational domain used in the Case III simulations of flow past a spill-through abutment. Shown are the main lengths (m) in the channel cross section.

The average mesh contained 2-3 million grid points, with the larger number corresponding to cases with a larger-width floodplain. Figure 4.3 visualizes the grid in relevant planes around the spill-through abutment. The gridding procedure was similar to that used for wing-wall abutments. The level of resolution of the boundary layers in the wall normal direction was also similar to that used for the wing-wall abutment cases. The velocity and length scales were also the same.

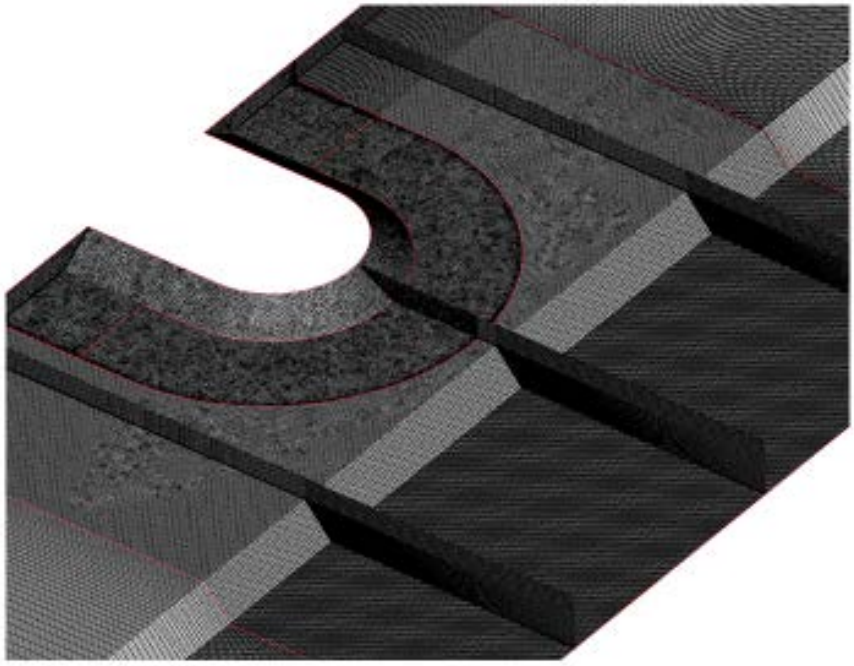

Figure 4.3 Computational grid used to mesh the channel containing a spill-through abutment for Case III simulations

Figure 4.4 visualizes the solution for Case IIIc1 for which B_f=1.4 m. The toe of the abutment is situated over the floodplain, well away from the interface between the floodplain and the main channel. The flow pattern at the free surface is quite different than the one observed for wing-wall abutments, where the extremity of the abutment protruded slightly into the main channel. As a result, the largest flow acceleration in the abutment region is observed some distance around the base of the abutment, close to the interface between the layer of riprap and the part of the floodplain covered by sand. The flow is greatly decelerated over the riprap layer due to the large roughness. A secondary, much smaller region of velocity amplification is observed very close to the upstream part of the extremity of the abutment. This is due to the acceleration of the incoming fluid moving close to the lateral wall containing the abutment and over the floodplain.

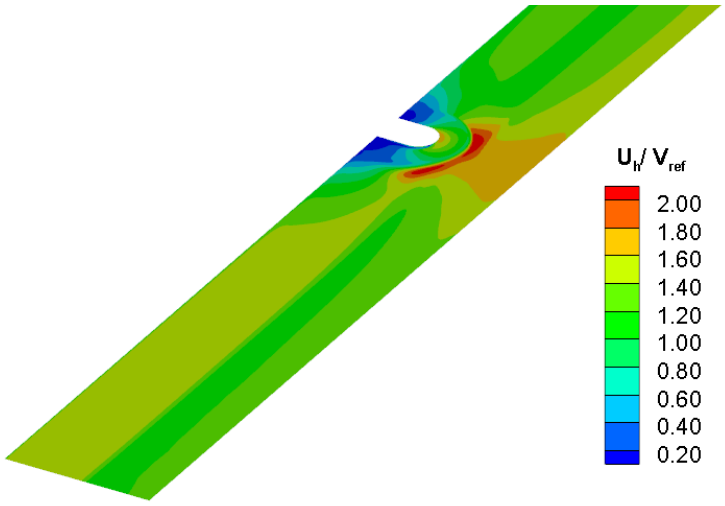
U_h / V_{ref}
2.00
1.80
1.60
1.40
1.20
1.00
0.80
0.60
0.40
0.20

a)

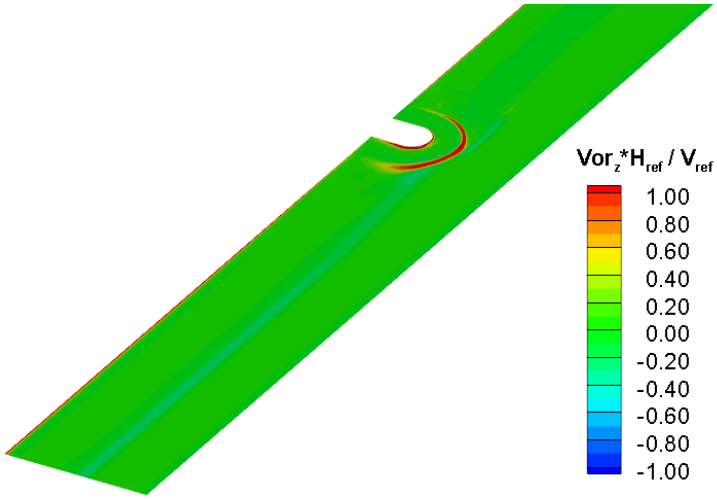
$Vor_z * H_{ref} / V_{ref}$
1.00
0.80
0.60
0.40
0.20
0.00
-0.20
-0.40
-0.60
-0.80
-1.00

b)

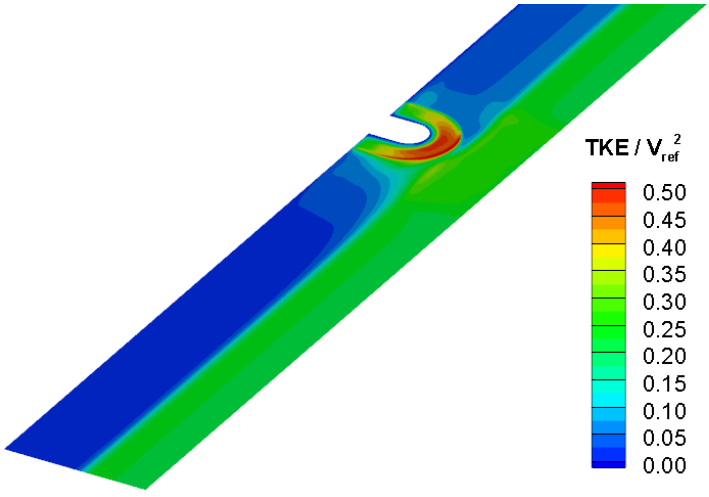
TKE / V_{ref}^2
0.50
0.45
0.40
0.35
0.30
0.25
0.20
0.15
0.10
0.05
0.00

c)

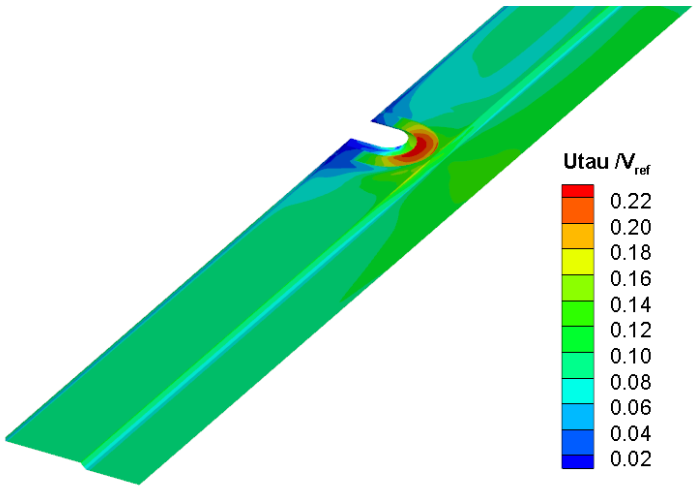

d)

Figure 4.4 Visualization of the solution for Case IIIc1 simulation with Fr=1.0. a) non-dimensional streamwise velocity at the free surface; b) non-dimensional vertical vorticity at the free surface; c) non-dimensional TKE; d) non-dimensional bed friction velocity.

At streamwise locations close to the abutment position, the velocity amplification occurring inside the main channel is important. The region of relatively high velocity amplification in the main channel extends until the left boundary of the computational domain. This means that lots of the fluid advected over the floodplain moves over the main channel as it passes the abutment. The velocity amplification over the sloped abutment boundary is relatively small.

The vertical vorticity contours at the free surface in figure 4.4b reveal the presence of two vorticity sheets close to the free surface. One is related to the separated shear layer originating close to the symmetry plane at the edge of the abutment, as the flow over the floodplain passes the extremity of the abutment. This separated shear layer remains in the vicinity of the downstream side of the abutment. However, the main vorticity sheet follows the outer edge of the region containing the riprap. It forms due to the large velocity difference between the faster

fluid moving over the sand region and the slower fluid moving over the riprap region. Consistent with this, the TKE distributions in figure 4.4c show that the largest amplification of the TKE occurs over the riprap region, in between the edge of the abutment and the edge of the riprap layer. The TKE values decay near the lateral wall containing the abutment. This is expected because the velocity magnitude is very small inside the recirculation regions. It is well known that the TKE levels are much larger in a turbulent boundary layer developing over a rough boundary compared to a smooth boundary.

The bed friction velocity distributions in figures 4.4d and 4.5 show the level amplification of the bed shear stress over the riprap region is comparable at locations situated close to the rounded edge of the abutment. This pattern is different from that observed for a wing-wall abutment. One should note that the bed friction velocity is much lower beneath the region of high velocity amplification situated away from the edge of the riprap region, both over the floodplain and over the main channel. This is mainly due to the much smaller values of the sand roughness covering these surfaces.

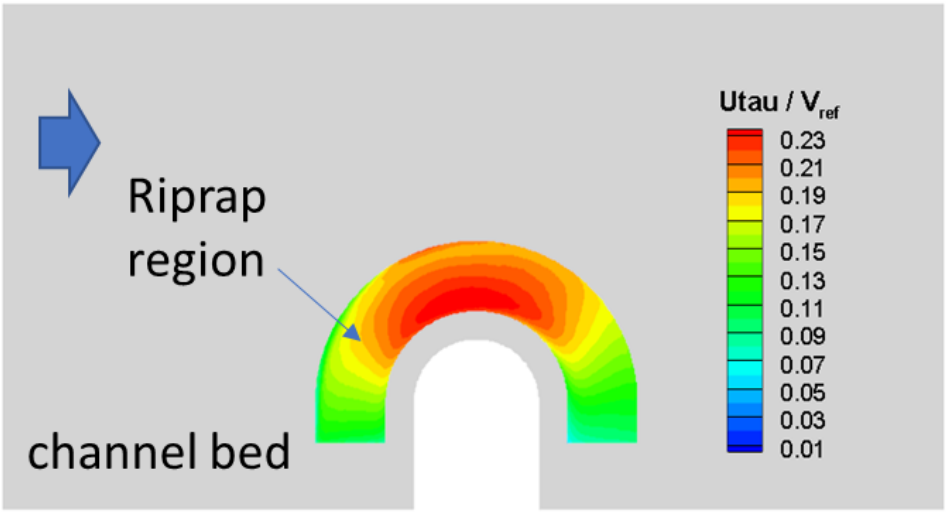

Figure 4.5 Nondimensional bed friction velocity distribution over the riprap layer predicted by the numerical simulation for the Case IIIc1 simulation with Fr= of spill-through abutment test cases.

4.2 Comparison with Predictions of Design Formulas

For spill-through abutments, the Froude number, Fr, was calculated using the mean velocity in the section containing the abutment, the flow depth in the main channel for cases with $L_a=B_f$ and the flow depth over the floodplain for abutments with $L_a<B_f$ and $(B_f-L_a)/y_m>5$ (HEC 23 recommendations).

For the Fr<0.8 cases, Lagasse et al. (2001) standard formula ($K_s=0.89$, $\alpha=2.0$) is fairly close to the numerical predictions but still not conservative enough for four of the test cases. Results in figure 4.6 show that using the equation recommended for Fr<0.8 until Fr~1 will result in a conservative design formula. The modified version of Lagasse et al. (2001) plotted in the previous figure results in conservative predictions of minimum riprap size. More data is needed to propose a modified design formula that will provide accurate estimations for Fr>0.8.

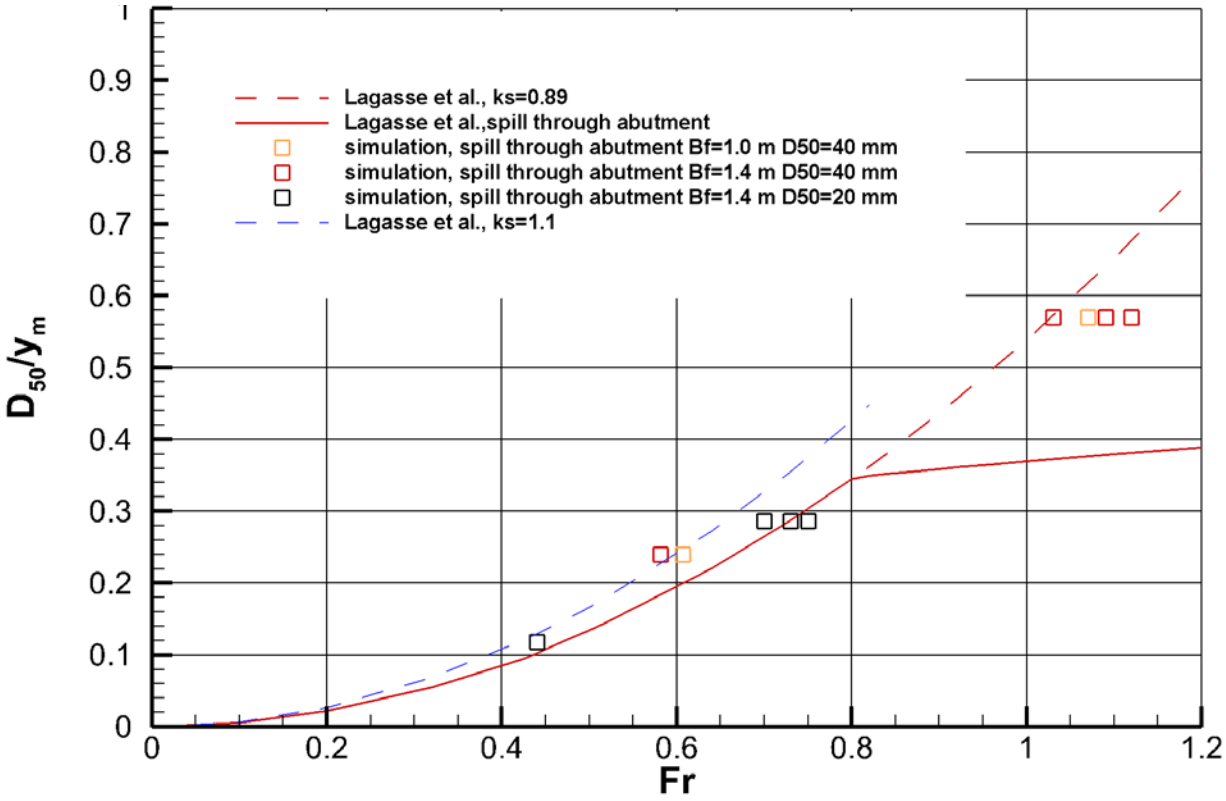

Figure 4.6 Comparison of numerical results with Lagasse et al. (2001) equation for spill-through abutments. Plotted is a modified version of Lagasse et al. (2001) formula (K_s=1.1)

Chapter 5 Conclusions, Recommendations, and Proposed Future Work

Reliable and safe transportation infrastructure design for flooding events is of great economic importance for state and federal agencies in charge of maintaining roads operational. Bridges are essential infrastructures that need to be protected against severe local scour around their piers and abutments during floods. More reliable design formulas for protection of bridge abutments against erosion will result in significant reduction of costs to operate roads during and after flood events. It will also reduce the risk for hazards associated with bridge failure during floods by avoiding structural failure.

As part of the present research, a general methodology based on 3-D RANS numerical simulations was developed to determine the conditions for riprap failure for cases when a riprap layer is placed close to an abutment or other hydraulic structure where local scour is a concern. The relationship proposed by Melville and Coleman (2000) and Melville et al. (2007) for riprap entrainment threshold (shear failure mode) was used to determine if riprap entrainment occurs. Such an approach is much less expensive and constraining compared to the classical one based on laboratory investigations conducted in a flume.

Fully 3-D RANS numerical simulations were conducted for a series of test cases. A wing-wall or spill-through abutment was placed in a straight channel containing a floodplain to obtain comprehensive information on how the conditions corresponding to the occurrence of riprap shear failure develop at such abutments as a function of the relative riprap mean diameter, main geometrical dimensions of the abutment and the channel, and the Froude number. Wing-wall abutments simulations were performed with different values of the riprap mean diameter and for two different flow depths corresponding to normal flow and flood conditions (flow over the floodplain). These test cases cover the main ones considered in the experimental laboratory

study of Melville et al. (2007). The numerical simulations were used to determine the distribution of the bed shear stress, vorticity, and TKE. Moreover, this database allowed validating the numerical approach based on comparison with experiments conducted for wing-wall abutments and further investigating the validity and predictive capabilities of the main design formula (Lagasse et al., 2001) in HEC 23 for this type of abutments. The database consisting of the 3-D RANS simulations was stored and is available for future use. These results are also needed as a base case against which one can investigate more complex cases, not covered by existing design recommendations (e.g., severe-flooding cases in which pressure scour effects are present, cases in which other flow training devices used to protect against bank erosion are present close to the abutment).

In the case of wing-wall abutments, the main recommendation is to modify the standard Lagasse et al. (2001) formula and use K_s=1.65 or, even better, to specify K_s as a function of the relative width of the floodplain (B_f/y_m) in HEC 23. This will allow the modified formula to fit most of the newly generated data. Based on the data set obtained for spill-through abutments, the recommended modification of the Lagasse et al. (2001) formula is to use K_s=1.1. This will ensure the design formula is conservative enough for all cases with Fr<0.8. Lagasse et al. (2001) standard formula (K_s=0.61, α=0.28) fails for the test cases with Fr>0.8. Another main result for spill-through abutments is the critical Froude number corresponding to the entrainment threshold decreases monotonically with increasing L_a/B_f or L_a/y_f (see series of test cases with constant $D_{50riprap}/y_m$ in fig. 4.6). This effect is ignored in present design formulas while being quite significant. Additional simulations are needed to quantify this effect and propose modifications in the design formula to account for it.

We also recommend performing a parametric study for $D_{50riprap}$=20 mm for spill through abutments, similar to that completed for $D_{50riprap}$=40 mm (B_f=0.5 m, 1.0 m, y_m=1.7 m, y_f=0.7 m with $0.3<L_a/B_f<1$), for cases where the toe of the spill-through abutment is situated far from the boundary of the main channel. These cases are listed in table 4.1. An additional series of simulations with B_f=2.0 m, y_m=1.7 m and 0.4 m$<L_a<$1.4 m can be used to check if the use of the Set Back Ratio method (see NCRHRP 24-23 and 24-18) recommended by HEC 23 results in accurate predictions of the riprap shear-failure entrainment threshold. The focus will be on cases where the velocity in the design formula is estimated as the ratio between the discharge over the floodplain and the floodplain part of the cross-sectional area in the abutment section.

Research would further improve from the investigation of the effect of bank curvature on erosion potential at wing-wall and spill-through abutments. The aim is to quantitatively understand how channel curvature amplifies the maximum bed shear stress over the riprap layer and then to propose a procedure based on the design formula of Lagasse et al. (2001) that will allow estimating the required size of the riprap stone needed to protect an abutment situated at the outer bank of a curved channel. The main idea is to modify the definition of the velocity in the contracted region and the shape factor in the original design formula of Lagasse et al. (2011) to obtain a conservative formula for such cases which are not covered by any design formula available in literature. These modifications would improve abutments placed in regions where bank curvature effects are significant.

We will work with the Transportation Research Board (TRB) committees related to bridges (e.g., TRB-AFB60) such that the main findings and the improved formulas will be considered for adoption in future releases of HEC 23. Once adopted by state and federal agencies in charge of maintaining operational bridges, the present research will increase the efficiency of

scour protection measures at two main types of abutments used especially for small bridges in the United States.

The proposed procedure described in the present report to estimate shear failure of riprap can be extended to other types of abutments and bridge piers of complex shape, or to cases when erosion at the abutment is due to more than one factor. Such cases are not covered by existing design formulas, which are mostly based on experiments conducted in straight channels. Given detailed information on the flow fields, turbulence and their effects on the bed shear stress distributions are available from these simulations, the present approach can lead to incorporating more physics into existing design formulas and proposing new design formulas for protection against local scour at hydraulic structures.

References

Cardoso, A., Simarro, G. and Schleiss, A. 2010. “Sizing of riprap for spill-through abutments,” *Water Management*, 163, issue WM10, 499-507, Paper 900024.

Cheng, Z., Koken, M. and Constantinescu, G. 2018. “Approximate methodology to account for effects of coherent structures on sediment entrainment in RANS simulations with a movable bed and applications to pier scour” *Advances in Water Resources*, in press

Ettema, R, Constantinescu, G and Melville, B. 2011. “NCHRP 24-27(01): Evaluation of bridge pier scour research: scour processes and estimation” Final report for NCHRP.

HEC-23 Bridge scour and Stream Instability Countermeasures [Lagasse, P, Zevenberger,L., Schall, J and Chopper, P (2001), ‘Bridge scour and stream instability countermeasures,’ *Rep. No. FHWA-NH1-01-003*, Hydraulic Engineering Circular No. 23, 2nd Ed. Office of Bridge Technology, Federal Highway Administration, Washington DC]

HEC-23 Bridge scour and Stream Instability Countermeasures: Experience. Selection and Design Guidance, 2009, 3rd Edition

Horna Munoz, D. and Constantinescu, G. 2016. “A numerical study of the efficiency of flood protection structures,” *International conference on fluvial hydraulics, River Flow 2016*, Saint Louis, USA.

Horna-Munoz, D. and Constantinescu, G. 2017. “Three dimensional numerical modeling of dam break flows,” *4th International Symposium of Shallow Flows*, Eindhoven University of Technology, The Netherlands, June 2017

Hoffmans, G. J. C. M. and Verheij, H. J. 1997. “Scour manual.” A.A. Balkema, Rotterdam, Netherlands.

Melville, B. W. and Coleman, S. E. 2000. ”Bridge scour.” Water Resources Publications, Littleton, Colorado.

Melville, B., van Ballegooy, S., Coleman, S. and Barkdoll, B. 2006a. “Countermeasures to protection at spill-through abutments,” *J. Hydr. Engrg.*, 132:235-245.

Melville, B., van Ballegooy, S., Coleman, S. and Barkdoll, B. 2006b. “Scour countermeasures for wing wall abutments,” *J. Hydr. Engrg.*, 132:563-574.

Melville, B., van Ballegooy, S., Coleman, S. and Barkdoll, B. 2007. “Riprap selection at wing wall abutments,” *J. Hydr. Engrg.*, 133:1265-1269.

NCHRP Project 24-18 (*NCHRP Report 587*), “Countermeasures to Protect Bridge Abutments from Scour”

NCHRP Project 24-19, “Selection Criteria and Design Guidelines, and techniques for the Size and Placement of Environmentally Sensitive Channel and Bank Protection Measures, and Quality Control”

NCHRP Project 24-20, “Prediction of Scour at Bridge Abutments”

NCHRP Project 24-23, “Riprap Design Criteria, Specifications,”

Pagaz-Ortiz, J. 1991. “Stability of rock riprap for protection at the toe of abutments located at the flood plain,” *Rep. No. FHWA-Rd-91-057*, Federal Highway Administration, US Dept. of Transportation, Washington, DC.

Sumer, B. M. and Fredsoe J. 2002. “The mechanics of scour in the marine environment.” World Scientific.